DOI: 10.1002/adfm.200800049

Supporting Information

Iron(II) metallomesogens exhibiting coupled spin state and liquid crystal phase transitions at room temperature

By *Maksym Seredyuk*, *Ana B. Gaspar**, *Vadim Ksenofontov*, *Yury Galyametdinov*, *Joachim Kusz*, and *Philipp Gütlich**

Table S1. Crystallographic data and refinement details for **C_6-1**.

Empirical formula	$C_{44}H_{66}Cl_2FeN_6O_{11}$
Formula weight	956.48
Temperature [K]	100.0(1)
Wavelength [Å]	0.71073
Crystal system	orthorhombic
Space group	*P*bca
a [Å]	18.746(4)
b [Å]	14.398(3)
c [Å]	36.174(7)
Volume [Å^3]	9763.54(347)
Z	8
ρ [g cm^{-3}]	1.335
Absorption coefficient [mm^{-1}]	0.481
F(000)	4159
θ range for data collection [°]	2.88 to 32.88
Index ranges	$-27 \le h \le 28$ $-9 \le k \le 21$

	$-53 \leq l \leq 53$
Reflections collected	16690
Independent reflections	7834
Data/restraints/parameters	16690/0/584
Goodness-of-fit, F^2	0.827
Final R indices [$I > 2\sigma(I)$]	$R1$ = 0.0456, $wR2$ = 0.1050
R indices (all data)	$R1$ = 0.1173, $wR2$ = 0.1158
ρ_{min}, ρ_{max} [e Å^{-3}]	1.938, -0.692

Table S2. MS, TGA and IR spectral data for complexes **C_n-1** and **C_n-2**.

Compound	**MS**[b]	**TGA, w/w [%]**	**IR [cm^{-1}]** [g]					
			ν(O–H)	$\nu_s(CH_2)$, $\nu_{as}(CH_2)$	*ν*(N=C)	*δ*(CH_2)	*ρ*(CH_2)	*ν*(Anion)
C_6-1	391 $[M]^{++}$ [c] 728 $[M+H]^+$ 881 $[M+ClO_4]^+$	0	–	2932, 2854	1626	1461	–	1084, 622
C_{18}-1	1387 $[M+ClO_4]^+$	0	–	2920, 2851	1630	1463	721	1087, 622
C_{10}-2	970 $[(M+F]^+$	0	–	2921, 2852	1647	1464	722	1069
C_{12}-2	1054 $[M+F]^+$	0	–	2921, 2852	1648, 1698	1467	721	1066
C_{14}-2	1206 $[M+BF_4]^+$	0	–	2919, 2851	1630, 1698	1466	721	1081
C_{16}-2	1289 $[M+BF_4]^+$	0	–	2918, 2850	1650	1468	721	1072
C_{16}-2[a]			–	2919, 2851	1650	1468	721	1072
C_{17}-2	1264 $[M+F]^+$ 1332 $[M+BF_4]^+$	0	–	2921, 2852	1648, 1699	1463	721	1081
C_{18}-2	644 $[M]^{++}$ 1375 $[M+BF_4]^+$	0	–	2918, 2850	1654, 1698	1467	721	1071
C_{20}-2 $\cdot H_2O$	1458 $[M+BF_4]^+$ 686 $[M]^{++}$	1.3	3410 br	2919, 2851	1645, 1697	1464	721	1076

[a] After the first heating up to 410 K; [b] Values of the peaks are given for the ions with the isotope ^{56}Fe; [c] Trace; [g] *ν*, stretching; *δ*, bending; *ρ*, rocking; *as*, asymmetric; *s*, symmetric

Figure S1. Variable temperature XRPD patterns of **C_{18}-1** (a), **C_{10}-2** (b), **C_{12}-2** (b), **C_{14}-2** (d), **C_{16}-2** (e), **C_{17}-2** (f), **C_{18}-2** (g) and **C_{20}-2** (h).

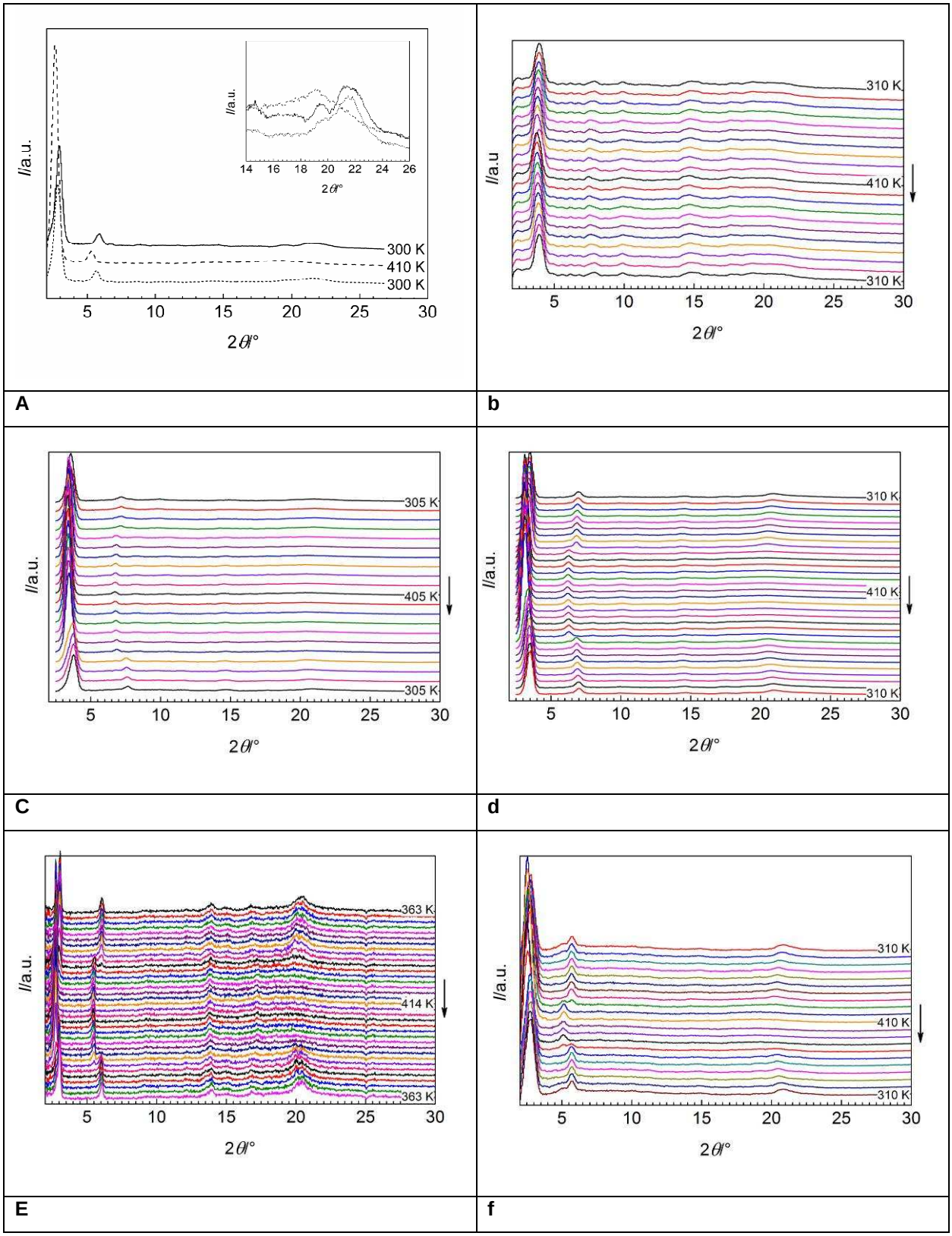

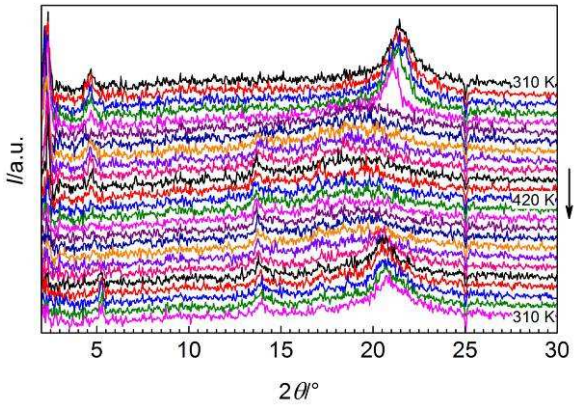 I/a.u. 310 K 420 K 310 K 5 10 15 20 25 30 2θ/°	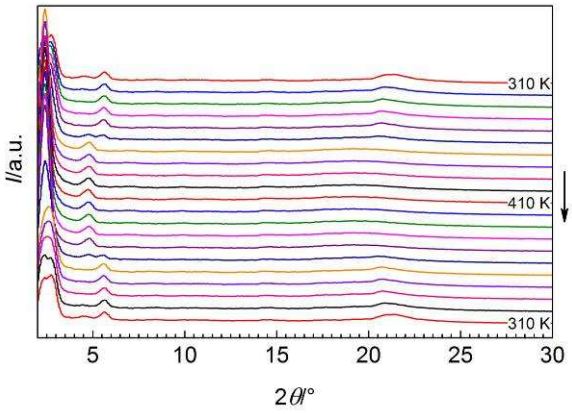 I/a.u. 310 K 410 K 310 K 5 10 15 20 25 30 2θ/°
G	**h**

Figure S2. Magnetic properties of compounds **C_6-1** (a), **C_{18}-1** (b), and **C_{10}-2** (c) in the form of $\chi_M T$ vs T.

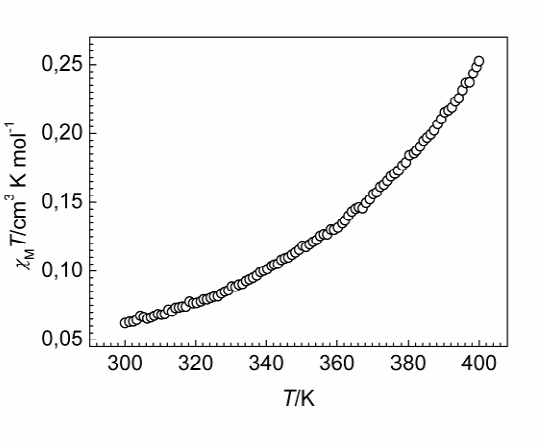

A

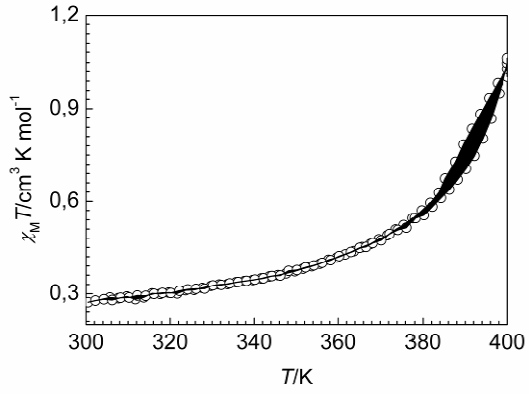

b

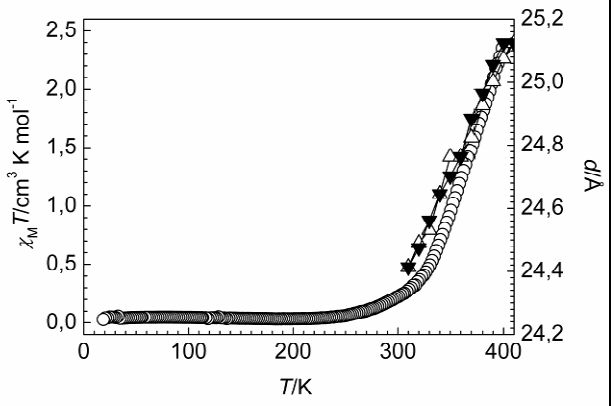

C

Figure S3. The solid and dashed lines represent the simulation of the transition curve of **C_{12}-2** using the Slichter-Drickamer model in the regions before and after melting.

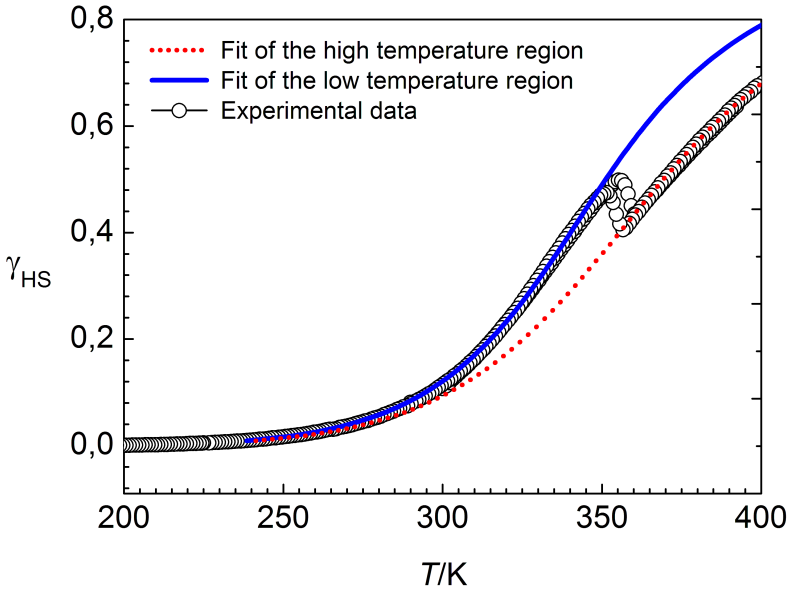

Figure S4. The anisotropic texture of compound **C_{16}-2** under crossed polarizers.

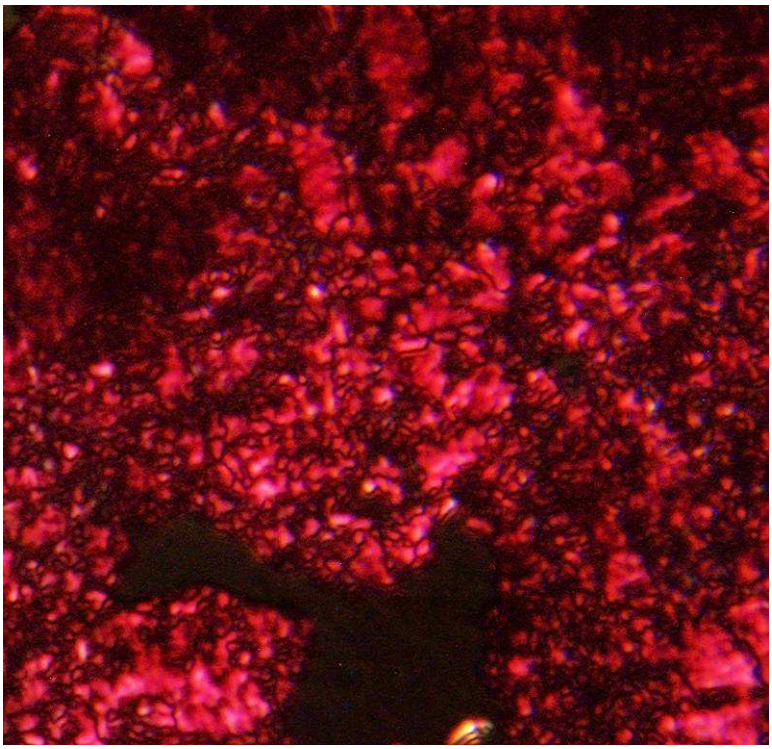

Figure S5. DSC measurements for **C_{18}-1** (a), **C_{10}-2** (b), **C_{12}-3** (c), **C_{14}-2** (d), **C_{16}-2** (e), **C_{17}-2** (f), **C_{18}-2** (g) and **C_{20}-2** (h) in heating and cooling modes at the rate of 10 K/ min. Arrows show direction of the scanning runs.

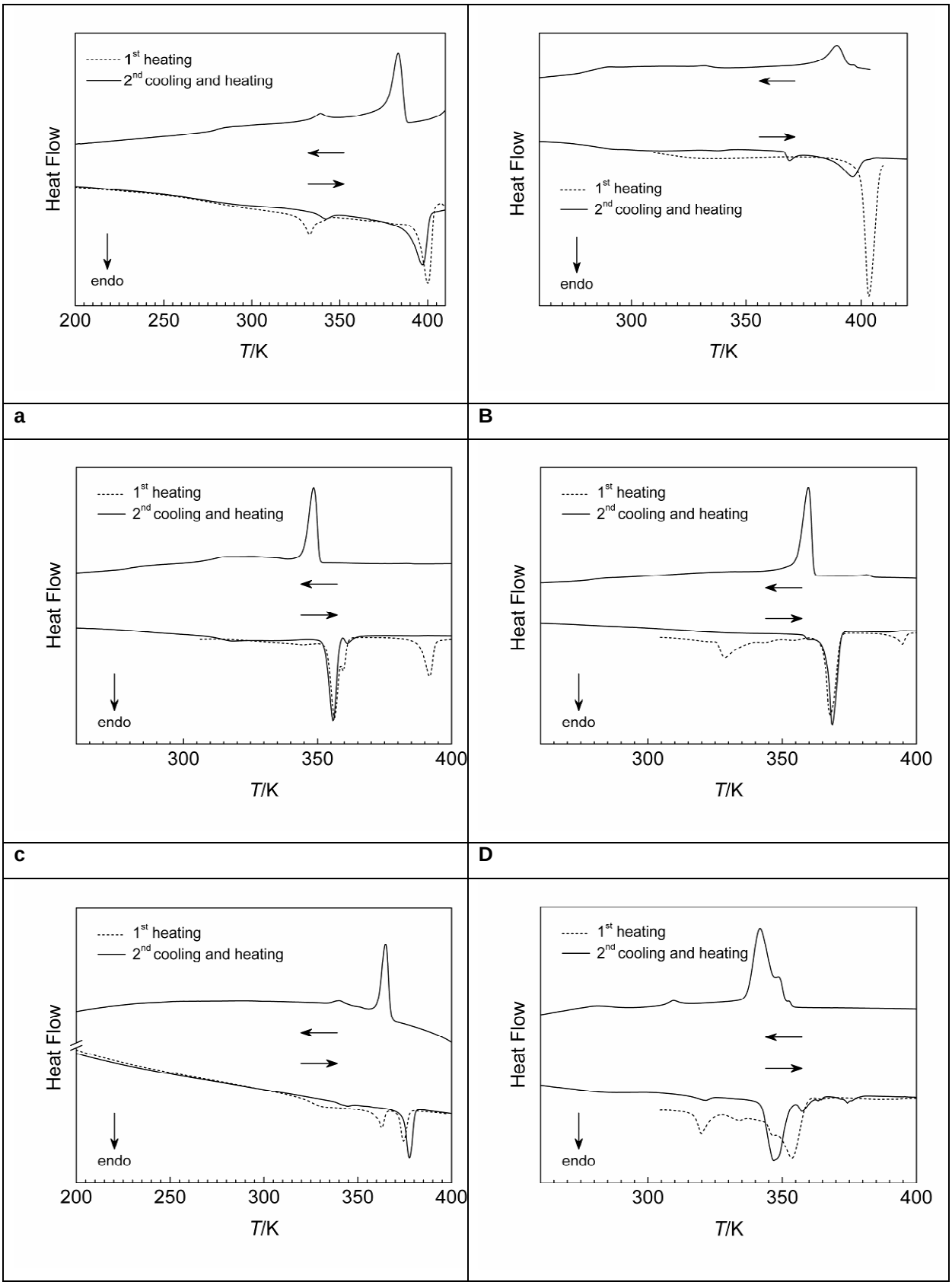

e	F
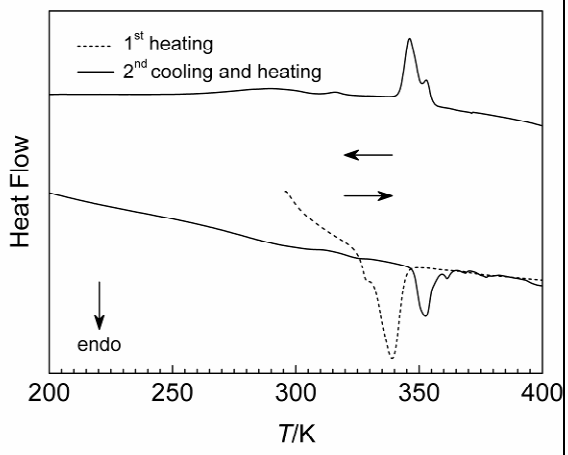 1st heating 2nd cooling and heating Heat Flow endo 200 250 300 350 400 T/K	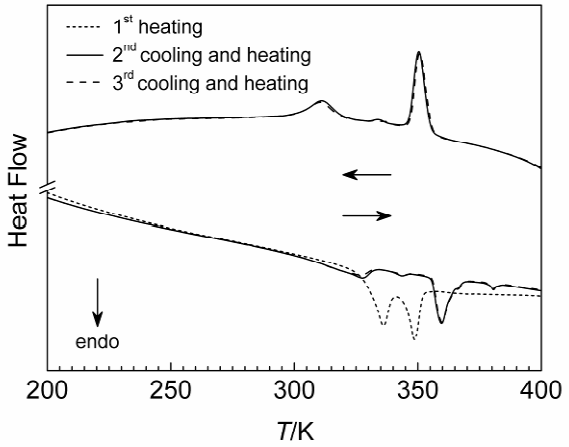 1st heating 2rd cooling and heating 3rd cooling and heating Heat Flow endo 200 250 300 350 400 T/K
g	**H**

Figure S6. Mössbauer spectra of compounds **C_6-1** (a), **C_{18}-1** (b), **C_{10}-2** (c), **C_{12}-2** (d), **C_{14}-2** (e), **C_{16}-2** (f), **C_{17}-2** (g), **C_{18}-2** (h) and **C_{20}-2** (i) measured at 80 K.

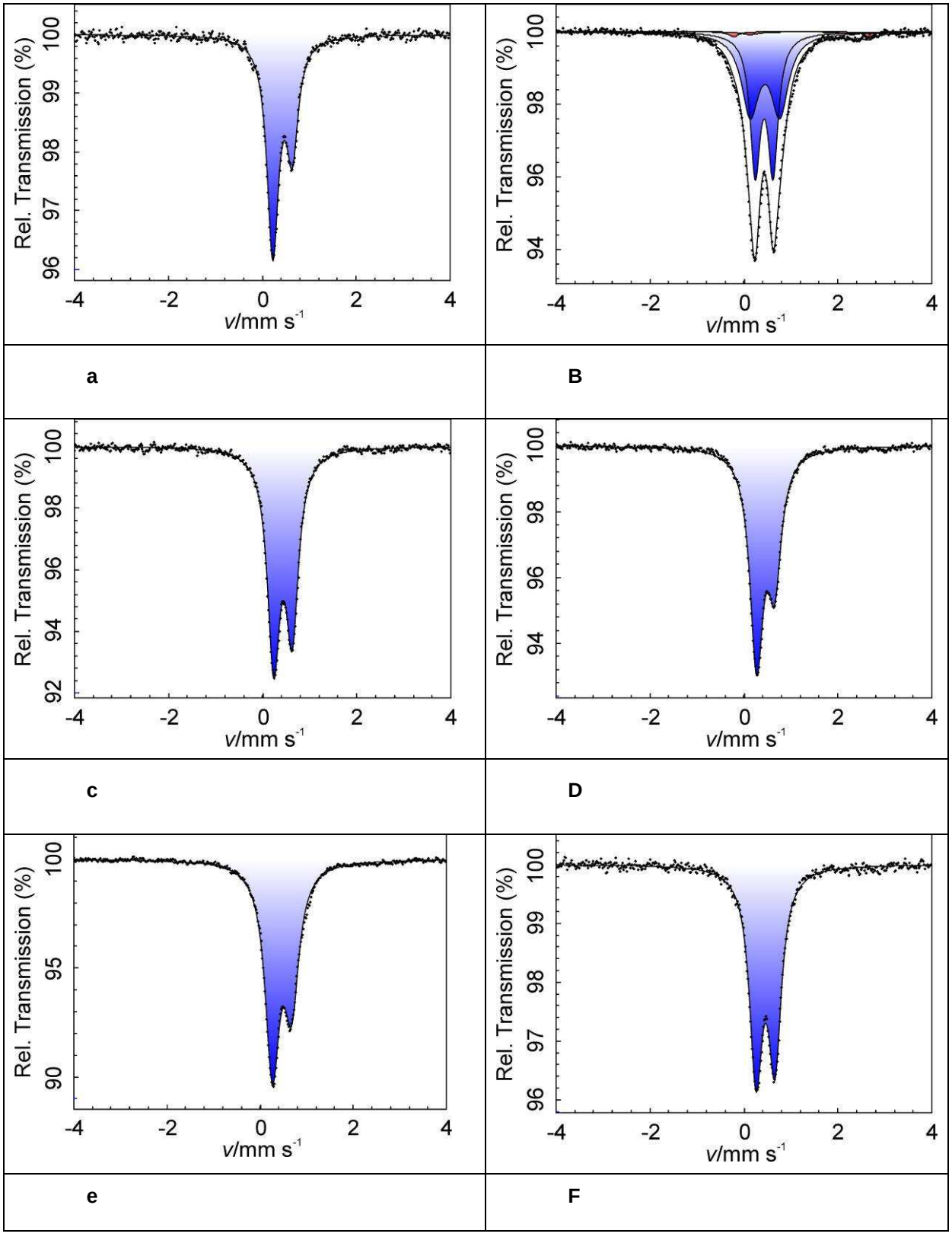

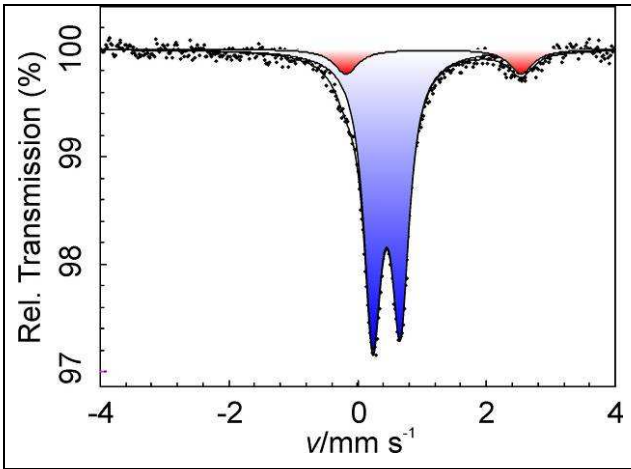
Rel. Transmission (%)
100
99
98
97
-4
-2
0
2
4
v/mm s-1

g

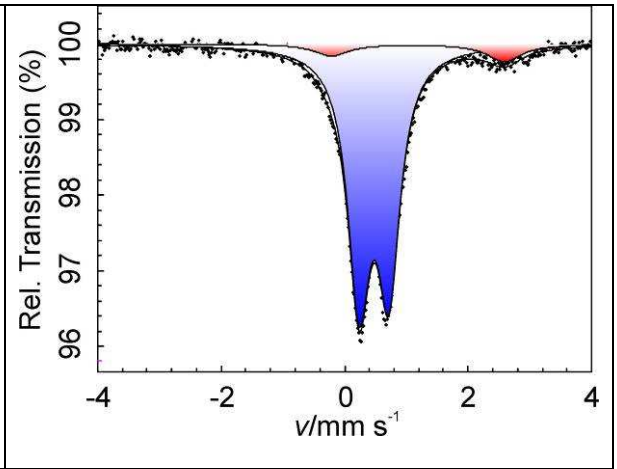
Rel. Transmission (%)
100
99
98
97
96
-4
-2
0
2
4
v/mm s-1

H

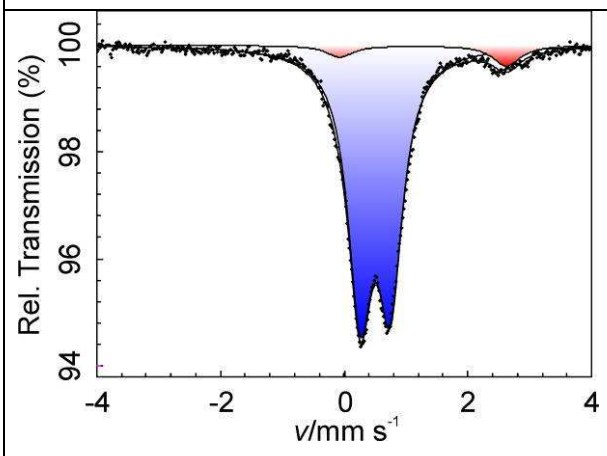
Rel. Transmission (%)
100
98
96
94
-4
-2
0
2
4
v/mm s-1

i

Table S3. Mössbauer parameters, isomer shift (δ, relative to α-iron), quadrupole splitting (ΔE_Q), half-width of the lines ($\Gamma_{1/2}$) and percentage of populations in the HS and LS states (A) for **C_n-1** (n = 6, 18), **C_n-2** (n = 10, 12, 14, 16, 17, 18, 20) at 80 K.

Compound	**Spin state**	**δ [mm s^{-1}]**	**ΔE_Q [mm s^{-1}]**	**$\Gamma_{1/2}$ [mm s^{-1}]**	**A [%]**
C_6-1	LS	0.43(2)	0.41(0)	0.15(1)	100
C_{18}-1	LS1	0.45(1)	0.38(1)	*0.13*	*47*
	LS2	0.45(1)	0.64(0)	*0.22*	*47*
	HS1	1.05(3)	2.58(7)	*0.13*	*3*
	HS2	1.26(3)	2.91(1)	*0.22*	*3*
C_{10}-2	LS	0.43(0)	0.39(0)	0.16(0)	100
C_{12}-2	LS	0.46(0)	0.38(0)	0.17(0)	100
C_{14}-2	LS	0.43(1)	0.40(0)	0.17(1)	100
C_{16}-2	LS	0.46(1)	0.40(0)	0.17(1)	100
C_{17}-2	LS	0.45(1)	0.43(1)	0.17(0)	88.5(16)
	HS	1.18(1)	2.72(1)	0.23(5)	11.5(24)
C_{18}-2	LS	0.48(1)	0.48(0)	0.22(0)	89.5(11)
	HS	1.22(5)	2.81(10)	0.37(8)	10.5(22)
C_{20}-2·H_2O	LS	0.50(0)	0.49(1)	0.24(0)	90.7(7)
	HS	1.32(0)	2.61(5)	0.29(4)	9.3(12)

The values given in italics were fixed during the fitting.

Figure S7. TGA analysis of compound **C_{20}-2**·H_2O.